International Journal of Heat and Mass Transfer 90 (2015) 15–25

Contents lists available at ScienceDirect

International Journal of Heat and Mass Transfer

journal homepage: www.elsevier.com/locate/ijhmt

Azimuthal instability modes in a viscoelastic liquid layer flowing down a heated cylinder

M. Moctezuma-Sánchez, L.A. Dávalos-Orozco *

Instituto de Investigaciones en Materiales, Departamento de Polímeros, Universidad Nacional Autónoma de México, Ciudad Universitaria, Circuito Exterior S/N, Delegación Coyoacán, 04510 México D. F., México

ARTICLE INFO

Article history:
Received 5 March 2015
Received in revised form 11 June 2015
Accepted 11 June 2015
Available online 26 June 2015

Keywords:
Thin liquid film
Thermocapillarity
Marangoni convection
Viscoelasticity
Cylindrical layer
Azimuthal modes

ABSTRACT

In this paper the non axisymmetric longwave instability of a thin viscoelastic liquid film flowing down a vertical heated cylinder is investigated. The stability of the film coating a cylinder in the absence of gravity is also investigated. In a previous paper it is found that viscoelasticity stimulates the appearance of azimuthal modes but the axial mode is the most unstable one. Other calculations in a former paper show that for flow outside a heated cylinder azimuthal modes can be the more unstable when the Marangoni number is large and, in particular, when the Reynolds number and wavenumber are small. Therefore, the small wavenumber and large cylinder radius approximation is assumed with the simultaneous action of viscoelasticity and thermocapillarity on the stability of azimuthal modes. In the presence and in the absence of gravity, it is found that, in comparison with the Newtonian case, it is easier to excite the azimuthal modes when viscoelasticity and thermocapillarity destabilize at the same time. Moreover, it is shown that, despite the axial mode is the most unstable one, there are wide wavenumber ranges where higher modes are the more unstable and they can show up by means of a periodic time dependent perturbation.

1. Introduction

The coating of surfaces by liquid films have important applications in industry. The problems found when looking for the perfect finishing are due to hydrodynamic instabilities. In the absence of gravity a cause of instability is thermocapillarity. When the liquid layer is coating a flat wall Pearson [1] has shown that a liquid film is unstable to temperature gradients perpendicular to the layer. As a consequence convection cells appear which may have important consequences in the solidified film. Therefore, it is necessary to investigate this instability under different mechanical and thermal boundary conditions. When the free surface is deformable the problem is investigated first by Scriven and Sternling [2]. The restoring influence of gravity is taken into account by Takashima [3] in the stationary case and by Takashima [4] when the flow is time dependent. The double diffusive Marangoni convection is first investigated by Mctaggart [5]. Sometimes in applications the fluid has elastic properties due to the presence in solution of macromolecules which change their form when shear stresses are applied to the liquid. These fluids are called viscoelastic (see for example Bird et al. [6]) and have been investigated widely in natural convection phenomena (see a recent review paper by Dávalos-Orozco [7–9] by Pérez-Reyes and Dávalos-Orozco). Notice that one characteristic of the viscoelastic instabilities is that they can be time dependent, in contrast to Newtonian fluids convection. Yet it is shown [8] that these instabilities do not occur for any thermal boundary conditions.

The thermal Marangoni instability has also been investigated for viscoelastic fluids by a number of authors. Getachew and Rosenblat [10] calculated the codimension-two points where stationary and oscillatory convection compete to be the first unstable one when the Marangoni number increases. Wilson [11] investigates supercritical conditions of the thermocapillary instability of a viscoelastic fluid from the point of view of the growth rates. Siddheshwar et al. [12] investigate the instability of a Maxwell fluid under different thermal boundary conditions including the effect of viscosity variation with temperature. The thermocapillary instability of a Maxwell viscoelastic fluid is investigated by Hernández-Hernández and Dávalos-Orozco [13] assuming a flat free surface and presenting results for a wide range of wall thermal conductivities. The goal is to calculate the codimension-two points where the stationary and oscillatory Marangoni convection modes compete to be the first unstable one.

* Corresponding author.
E-mail address: ldavalos@unam.mx (L.A. Dávalos-Orozco).

http://dx.doi.org/10.1016/j.ijheatmasstransfer.2015.06.035
0017-9310/

Nomenclature

Bi	free surface-atmosphere Biot number
c	phase velocity
Cr	crispation number
De	Deborah number
$\mathbf{e}$	shear rate tensor
g	acceleration of gravity
h	free surface deformation
h_0	mean thickness of the layer
H_h	heat transfer coefficient
H	free surface perturbation amplitude
k	axial wavenumber
k_C	critical wavenumber
k_f	fluid thermal conductivity
L_1	adimensional relaxation time
L_2	adimensional retardation time
m	azimuthal number
Ma	Marangoni number
$\overrightarrow{n}$	normal vector
P	pressure
$p_i : i$-th	order perturbation pressure
Pr	Prandtl number
R	cylinder radius
Re	reynolds number
S	surface tension number
$\overline{S}$	scaled surface tension number
$\overline{T}$	temperature
T_{amb}	ambient temperature
$T_i : i$-th	order perturbation temperature
T_W	wall temperature
U	representative velocity
$\overrightarrow{V}$	velocity vector
We	Weber number

Greek

α	fluid thermal diffusivity
β	non dimensional cylinder radius
γ	surface tension
δ	scaled non dimensional cylinder radius
ΔT	temperature difference
ρ	fluid density
ν	kinematic viscosity
σ	growth rate
τ	shear stress tensor
$\overrightarrow{\tau_1}$	first tangential vector
$\overrightarrow{\tau_2}$	second tangential vector
ω	frequency of oscillation

When a fluid layer flows down a wall, the thermocapillary effects are included by Joo et al. [16,14] and Ramaswamy et al. [15]. A complete review of this problem is found in Dávalos-orozco [17].

Nonlinear computations of the instability of a thin viscoelastic film falling down an inclined wall are done by Joo [18]. Kang and Chen [19] find in the linear limit a purely elastic instability. This flow is investigated by Dávalos-Orozco [20] when the wall is smoothly deformed. It is shown that it is still possible to stabilize the flow by means of spatial resonance as done by Dávalos-Orozco [21] when the fluid is Newtonian.

It is of interest to know if the azimuthal modes are relevant in a cylindrical wall. Shlang and Sivashinsky [22] found that the azimuthal modes can not be the most unstable in a Newtonian fluid and that the axial one is always the most unstable one. For flow inside the cylinder the axial mode grows faster as in microchannels when the liquid forms an annular film [23,24]. Therefore, for any radius, the axial mode is the most unstable one inside the cylinder. When a film is flowing down the outside of a rotating cylinder, it has been shown [25–27] that the first azimuthal mode may be the most unstable one under different circumstances. Nevertheless, for flow inside the cylinder (as in [28]) the most unstable mode is the axial one. The relevance of the azimuthal modes is also found in the instability of inviscid stratified fluids in a rotating annulus [29].

The thermocapillary phenomena of a film flowing down a vertical cylinder present interesting results. This free surface condition is of concern in practical applications of heat dissipation [30]. Linear stability calculations of a thin film flowing down a cylindrical heated wall (see Dávalos-Orozco and You [31]) have demonstrated that high azimuthal modes can be the more unstable ones when the Reynolds number and the wavenumber of the perturbation are small. To excite these modes large magnitudes of the temperature gradient are required. It is important to point out that in the presence of thermocapillarity, the azimuthal modes can also be excited as the more unstable ones when the flow is inside the cylinder.

The two dimensional flow instability of non-Newtonian thin films flowing down a cylinder has also been investigated by Cheng and Liu [32–34] for a power-law fluid, by Cheng et al. [35] and Cheng and Lai [36] for a viscoelastic Walters B fluid (with application to magnetohydrodynamics). In Moctezuma-Sánchez and Dávalos-Orozco [37] the viscoelastic Oldroyd's constitutive equation model was used to investigate the longwave linear instability of a fluid film flowing down a cylinder. The corresponding linear equation reduces to that obtained by Joo [18] (without power-law fluid effects) when the radius of the cylinder tends to infinity. In particular, the interest in [37] is to determine the relevance of the azimuthal modes in the presence of viscoelasticity. It is found that the most unstable mode is always the axial one. Eventhough, viscoelasticity promotes the appearance of the azimuthal modes in comparison with the Newtonian fluid, they are not the more unstable ones in any range of the wavenumber.

In the present paper, the interest is focused on the thermocapillary excitation of azimuthal modes in a viscoelastic fluid. A comparison is done with the results of the isothermal [37] flow and the Newtonian fluid [31] flow. The Oldroyd's fluid model is selected for the constitutive equation of the fluid. The linear evolution equation calculated below, reduces to that of Joo [18] when the radius of the cylinder tends to infinity and in the absence of thermocapillary effects. In the lack of thermocapillary effects the equation reduces to that in [37]. The results of this paper are new not only because of the combination of viscoelasticity [37] and thermocapillarity [31] in flow on the surface of a cylinder, but also because the problem investigated is three dimensional. This can be seen in the review section on thin film flow down cylinders presented in Dávalos-orozco [17]. It is found that in the linear and non linear problems, mainly axial mode stability is investigated. For three dimensional flows see [22,25–27,29]. The physical reason for the appearance of azimuthal modes of instability are the azimuthal shear stresses created by thermocapillarity, as will be seen presently in the discussion of the first and second tangential shear stresses of the free surface boundary conditions.

The paper is organized as follows. The equations of motion and boundary conditions are presented in the next section. The numerical results are given in Sections 3 for zero Reynolds number and 4 for a film flowing down a cylinder. The last Section 5 are the conclusions.

2. Viscoelastic fluid layer flowing down a heated cylinder

In this section, the equations of motion of a thin viscoelastic fluid film flowing down the outside of a heated cylinder are presented. It is assumed that the axis of the cylinder is vertical and that the z-axis is in the direction of the gravity vector. The wall of the cylinder is supposed to be a very good conductor. The liquid is in contact with an inviscid atmosphere which has at the interface particular heat transfer properties. The free surface is susceptible to shear stresses and deformation due to thermal perturbations leading to thermocapillary effects.

The fluid film has density ρ, kinematic viscosity v, thermal conductivity α and a mean thickness h_0. The equations of motion, mass conservation and heat diffusion are made non dimensional along with the constitutive equation using $U = gh_0^2/2v$ for the velocity, h_0 for the coordinates r and z, h_0/U for time and ρU^2 for the pressure and shear stress tensor. Here g is the acceleration of gravity. The temperature is made non dimensional by means of $\Delta T = T_W - T_{amb} > 0$, where T_W is the temperature of the cylindrical wall and T_{amb} is the temperature of the inviscid ambient atmosphere.

The governing equations of a heated viscoelastic Oldroyd fluid layer are the balance of momentum, heat diffusion and continuity equations in cylindrical coordinates. In non dimensional form they are:

$$\frac{d\vec{V}}{dt} = -\nabla P + \nabla \cdot \tau + \frac{2}{Re}\hat{k} \tag{1}$$

$$\frac{d\overline{T}}{dt} = \frac{1}{RePr}\nabla^2 \overline{T} \tag{2}$$

$$\nabla \cdot \vec{V} = 0 \tag{3}$$

where $\vec{V}$ is the velocity vector, $\overline{T}$ is the temperature and $\hat{k} = (0, 0, 1)$ in cylindrical coordinates is a unit vector in the direction of gravity (z-direction). The shear stress tensor τ and the shear rate tensor $\mathbf{e} = (1/2)(\nabla\vec{V} + (\nabla\vec{V})^T)$ satisfy the Oldroyd's constitutive equation for a viscoelastic fluid. That is:

$$\tau + L_1 \frac{\mathcal{D}\tau}{\mathcal{D}t} = \frac{2}{Re}\left(\mathbf{e} + L_2 \frac{\mathcal{D}\mathbf{e}}{\mathcal{D}t}\right) \tag{4}$$

Here, the time operator is defined as $d/dt = \partial/\partial t + \vec{V} \cdot \nabla$. Besides, $\mathcal{D}/\mathcal{D}t$ is a nonlinear operator which could be the upper convected, the lower convected or the corotational time derivatives, depending on the viscoelastic model selected. Nevertheless if the equations are linearized around a basic hydrostatic state in the absence gravity, all the derivatives are the same as the linear operator $\mathcal{D}/\mathcal{D}t = \mathrm{d}/\mathrm{dt} = \partial/\partial t$. $Pr = v/\alpha$ is the Prandtl number, $Re = \mathrm{U}\ h_0/v$ is the Reynolds number and L_1 and L_2 are the non dimensional relaxation and retardation times of the viscoelastic fluid.

Let $\beta = R/h_0$ be the non dimensional radius of the cylinder (see Fig. 1). The boundary conditions are:

$$\vec{V} = 0, \qquad \overline{T} = 1 \qquad \text{at} \qquad r = \beta \tag{5}$$

$$(P_{amb} - P)\vec{n} + We\,\vec{n}\nabla \cdot \vec{n} = -\tau \cdot \vec{n} - \frac{Ma}{PrRe^2}\nabla\overline{T}$$
$$\text{at} \qquad r = \beta + h(\theta, z, t) \tag{6}$$

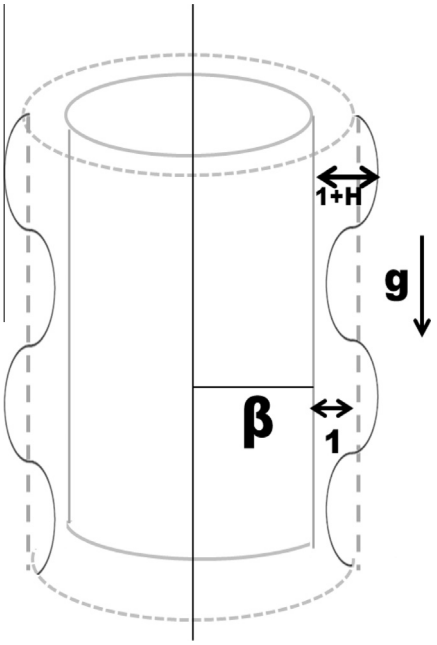

Fig. 1. Sketch of the system in nondimensional form. A viscoelastic liquid layer coating a vertical cylindrical wall. Gravity may be zero or different from zero.

$$-\vec{n} \cdot \nabla\overline{T} = Bi\overline{T} \qquad \text{at} \qquad r = \beta + h(\theta, z, t) \tag{7}$$

Here, $We = \gamma/\rho h_0 U^2$ is the Weber number with γ the surface tension, $Ma = -d\gamma/d\overline{T}\Delta T h_0/\rho\alpha v$ is the Marangoni number with α the fluid heat diffusivity, $Bi = H_h/k_f h_0$ is the Biot number with H_h the heat transfer coefficient and k_f the fluid heat conductivity. Notice that the gradient of the surface tension $\nabla\gamma = (d\gamma/d\overline{T})\nabla T$ depends on the temperature gradient and that $d\gamma/d\overline{T} < 0$ in common fluids. The height of the free surface is $h(\theta, z, t) = 1 + H(\theta, z, t)$ and $H(\theta, z, t)$ is the free surface perturbation amplitude. The normal and tangential vectors at the free surface of the liquid viscoelastic film on the cylindrical wall are defined as follows.

$$\vec{n} = \frac{(1, -\frac{1}{r}h_\theta, -h_z)}{\sqrt{1 + \frac{1}{r^2}h_\theta^2 + h_z^2}} \tag{8}$$

$$\vec{\tau_2} = \frac{(h_z, 0, 1))}{\sqrt{1 + h_z^2}} \tag{9}$$

$$\vec{\tau_2} = \frac{\left(-\frac{1}{r}h_\theta, -\left(1 + h_z^2\right), \frac{1}{r}h_\theta h_z\right)}{\sqrt{\left(1 + h_z^2\right)\left(1 + \frac{1}{r^2}h_\theta^2 + h_z^2\right)}} \tag{10}$$

The subscripts θ and z mean partial derivatives. $\vec{n}$ is the normal vector and $\vec{\tau_1}$ and $\vec{\tau_2}$ are the first and second tangential vectors. From Eq. 8 it is possible to calculate the curvature of the free surface defined by $\nabla \cdot \vec{n}$.

Now the variables in the equations and boundary conditions are scaled using $t \to \varepsilon t, z \to \varepsilon z, y = \delta\theta$ with $\delta = \varepsilon\beta$ (which means that the radius is assumed to be large). Here ε is a scaling parameter representing the thickness of the fluid layer over the perturbation wavelength. Besides, $H \to \varepsilon H$ (see reference [38]). If the fluid is assumed to have very strong surface tension, then the scaling extends to the definition $We = \gamma/\rho h_0 U^2 = \varepsilon^2 S/3Re^2$, where $S = 3\gamma h_0/\varepsilon^2\rho v^2$ is the surface tension number. Assuming that $\vec{V} = (u, v, w)$, the variables are expanded as:

$$u = \varepsilon(u_0 + \varepsilon u_1 + \cdots), \quad v = \varepsilon(v_0 + \varepsilon v_1 + \cdots),$$
$$w = w_0 + \varepsilon w_1 + \cdots, \tag{11}$$

$$P = p_0 + \varepsilon p_1 + \cdots, \qquad \overline{T} = T_0 + \varepsilon T_1 + \cdots \tag{12}$$

These expansions are introduced into the equations and boundary conditions. The problem is solved for each order of the expansions and finally at first order in the expansions the following linear partial differential equation is obtained for the free surface perturbations on a thin film flowing down the outside of a cylindrical vertical wall:

$$H_t - 2H_z + \varepsilon\left[-\frac{2}{3\delta}H_z + \frac{8}{15}ReH_{zz} + DeH_{zz} + \frac{1}{3}\frac{\overline{S}}{Re}\left(\frac{1}{\delta^2}\nabla_\perp^2 H + \nabla_\perp^4 H\right) + \frac{1}{2}\frac{Ma}{RePr}\frac{Bi}{(1+Bi)^2}\nabla_\perp^2 H\right] = 0 \tag{13}$$

where $De = 4(\lambda_1 - \lambda_2)v/3h_0^2$ is the Deborah number, $\overline{S} = \varepsilon^2 S$ and $\nabla_\perp = (\partial/\partial y, \partial/\partial z) = (\partial/\delta\partial\theta, \partial/\partial z)$.

It is also of interest in this paper to calculate the equation of the linear free surface perturbations of a thin film coating the outside of a cylindrical wall in the absence of gravity. To attain this goal, the following changes can be done in Eq. 13 (see also [31]). First, the term $8ReH_{zz}/15$ has to be zero. Second, the velocity is made non dimensional with $U = \alpha/h_0$. In this way the parameter $ReWe = 1/Cr$, where $Cr = \rho\alpha v/\gamma h_0$ is the crispation number. In other places where Re appears it changes into $1/Pr$. The equation is:

$$H_t - 2H_z + \varepsilon\left[-\frac{2}{3\delta}H_z + \frac{De}{Pr}H_{zz} + \frac{1}{3}\frac{1}{Cr}\left(\frac{1}{\delta^2}\nabla_\perp^2 H + \nabla_\perp^4 H\right) + \frac{1}{2}Ma\frac{Bi}{(1+Bi)^2}\nabla_\perp^2 H\right] = 0 \tag{14}$$

In this non dimensional form the Prandtl number appears explicitly in the viscoelastic term dividing De. The stability of these two cases will be discussed separately beginning with the case in the absence of gravity.

3. Thermocapillary convection of a film coating a cylinder

In this section the goal is to present the numerical results corresponding to the thermocapillary instability of a liquid film coating the outside of a cylinder in the absence of gravity. The perturbations are assumed to have the form of normal modes as $H = H_0 \exp[i(m\theta + kz + \omega t) + \sigma t]$. From now on it is assumed that $\varepsilon = 1$. This is substituted into Eq. 14 to get the equations for the phase velocity $c = \omega/k$, the growth rate and the critical wavenumber k_C. They are:

$$c = 2 + \frac{2}{3\delta}. \tag{15}$$

$$\sigma = \frac{De}{Pr}k^2 + \frac{1}{3Cr}\left(\frac{m^2}{\delta^2} + k^2\right)\left[\frac{1}{\delta^2} - \left(\frac{m^2}{\delta^2} + k^2\right) + \frac{1}{2}Ma\frac{Bi}{(1+Bi)^2}\right]. \tag{16}$$

$$k_C^2 = -\frac{m^2}{\delta^2} + \frac{3Cr}{2}\left(\zeta + \sqrt{\zeta^2 - \frac{4}{3Cr}\frac{De}{Pr}\frac{m^2}{\delta^2}}\right). \tag{17}$$

where $\zeta = De/Pr + 1/3Cr\delta^2 + MaBi/2(1+Bi)^2$. The critical wavenumber is obtained taking the square root of Eq. 17. The phase velocity decreases with the radius of the cylinder but the behavior of the growth rate in Eq. 16 is not clear due to the number of parameters involved. Here the Biot number will be fixed to $Bi = 0.1$. Graphics of the growth rate are given for two magnitudes of De/Pr and two of the radius of the cylinder. The crispation number Cr and the azimuthal mode number m are varied in each plot.

It can be shown analytically that mode $m = 0$ is always the most unstable one. However, here it will be demonstrated that when the wavenumber is very small the azimuthal modes can become the more unstable and that the number of modes increases with De and Ma. In other words, viscoelasticity and thermocapillarity promote the appearance of azimuthal modes as the more unstable in some regions of the wavenumber.

The results are presented fixing δ and De/Pr and varying the other parameters involved. In all the figures the numbers attached to the curves indicate the corresponding azimuthal modes. In Fig. 2 for the growth rate against the perturbation wavenumber, $\delta = 5$ and $De/Pr = 0.01$. The curves correspond to different crispation numbers as follows: solid: $Cr = 0.001$, dotted: $Cr = 0.01$, dashed: $Cr = 0.1$. The smaller crispation number corresponds to the stronger surface tension. The Marangoni number differs in each figure:

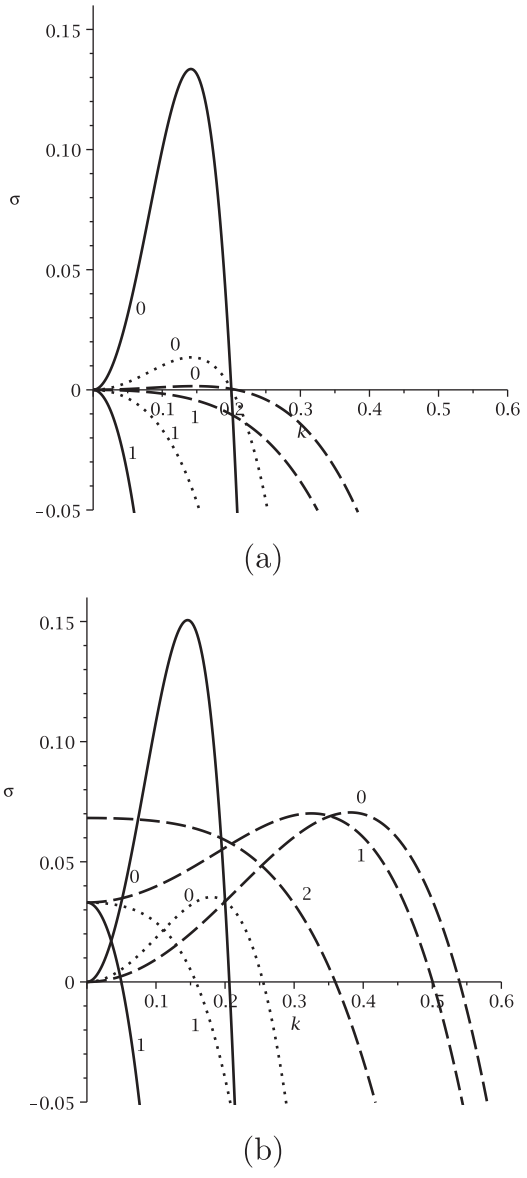

Fig. 2. σ vs k. $Re = 0$. $\delta = 5$, $De/Pr = 0.01$, $Bi = 0.1$. Fig. 2a $Ma = 0$, Fig. 2b $Ma = 20$. Solid: $Cr = 0.001$, dotted: $Cr = 0.01$, dashed: $Cr = 0.1$. The numbers are the azimuthal modes.

Fig. 2a $Ma = 0$ and Fig. 2b $Ma = 20$. The other figures have a similar explanation but with different δ and De/Pr.

The viscoelastic effects are small in this case. Clearly, the smallest crispation number has the largest growth rate due to the throttling effect of surface tension and the curves of $Cr = 0.001$ and mode $m = 0$ are very similar for the three Marangoni numbers used. However, note that $m = 1$ has important changes with $Ma > 0$ and that it is the more unstable mode in a range of the wavenumber. For the other crispation numbers, the growth rates of $m = 0$ and 1 have notable changes with Ma. As can be seen, increasing Ma higher azimuthal modes are able to appear as the more unstable ones in a larger range of the wavenumber. Observe that in Fig. 2a for $Ma = 0$ the first and higher azimuthal modes have no wavenumber region as the more unstable ones. In Fig. 3 shown are the curves of criticality, calculated from Eq. 17, for different parameters and azimuthal modes. It is seen the important increase of the critical wavenumber with Ma when the crispation number increases. This leads the wavenumber to a region outside the small wavenumber approximation. That is, to a stronger surface tension corresponds a lower wavenumber of the perturbation, even for large Marangoni numbers.

Fig. 4 shows results for a larger $De/Pr = 0.2$. It was shown [37] in the isothermal case that viscoelasticity promotes the increase of the growth rate and the appearance of higher azimuthal modes. This can be appreciated in the figure, where the growth rates are larger than those of Fig. 2. The differences are not clear for mode $m = 0$ of $Cr = 0.001$ whose change is very small. The change is more apparent in the dashed curves corresponding to $Cr = 0.1$. In this case, the growth rate is larger for modes $m = 0$ and 1 but not for $m = 2$, as seen in Fig. 4b. As can be seen, the Deborah number has no influence on the wavenumber of the intersection point. The reason is that when subtracting the growth rates of the intersecting modes the Deborah number disappears from the equation of k.

The critical wavenumber against Ma is shown in Fig. 5 where the growth of the curves is more steep than in Fig. 3. The difference is remarkable in the dashed curves for $Cr = 0.1$. The critical wave number approaches faster to the small wavenumber approximation limit with an increase of Ma.

The growth rates decrease considerably when the radius of the cylinder increases to $\delta = 10$. Nevertheless, this brings the possibility to have higher azimuthal modes as the more unstable ones. In Fig. 6a it is shown that in the isothermal case the unstable wavenumber region is considerably reduced in comparison with previous figures. Still, the increase in Marangoni number widens this range as seen in Fig. 6b when Cr increases.

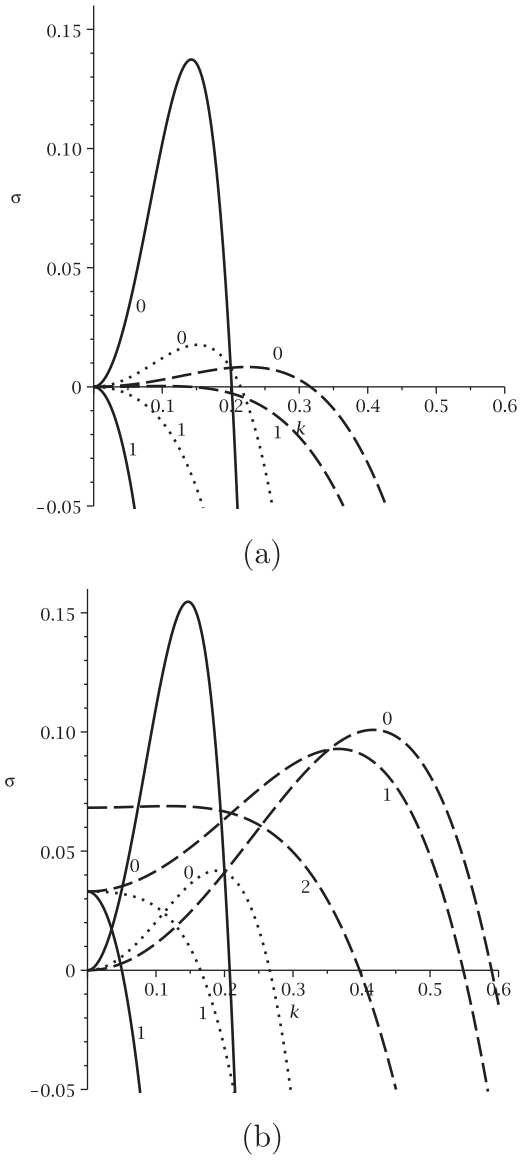

Fig. 4. σ vs k. $Re = 0$. $\delta = 5$, $De/Pr = 0.2$, $Bi = 0.1$. Fig. 4a $Ma = 0$, Fig. 4b $Ma = 20$. Solid: $Cr = 0.001$, dotted: $Cr = 0.01$, dashed: $Cr = 0.1$.

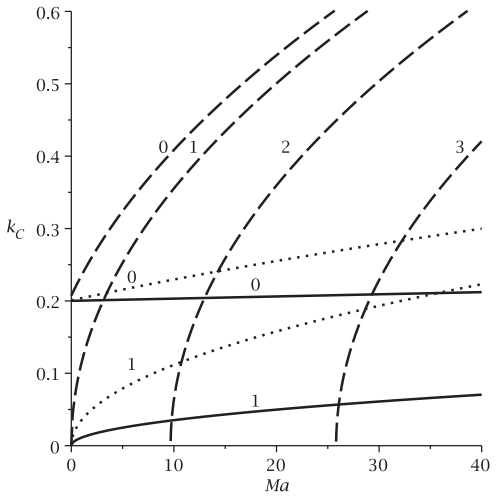

Fig. 3. k_C vs Ma. $Re = 0$. $\delta = 5$, $De/Pr = 0.01$, $Bi = 0.1$. Solid: $Cr = 0.001$, dotted: $Cr = 0.01$, dashed: $Cr = 0.1$.

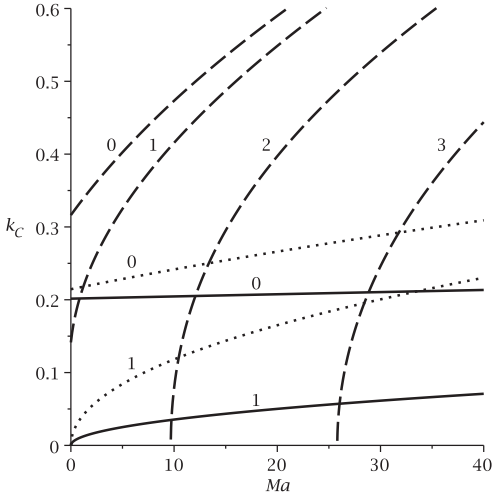

Fig. 5. k_C vs Ma. $Re = 0$. $\delta = 5$, $De/Pr = 0.2$, $Bi = 0.1$. Solid: $Cr = 0.001$, dotted: $Cr = 0.01$, dashed: $Cr = 0.1$.

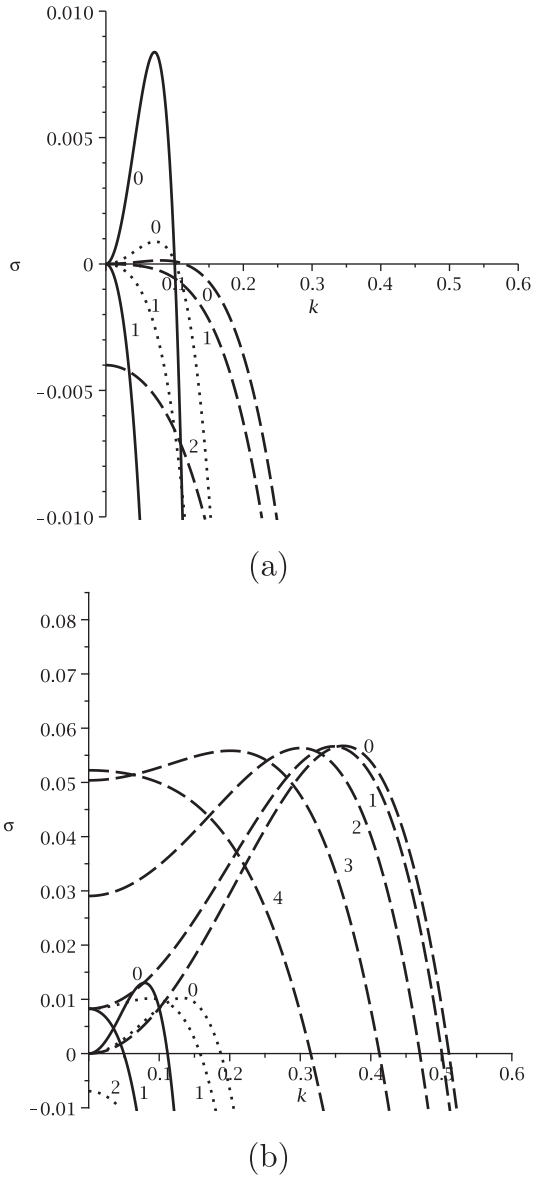

Fig. 6. σ vs k. $Re = 0$. $\delta = 10$, $De/Pr = 0.01$, $Bi = 0.1$. Fig. 6a $Ma = 0$, Fig. 6b $Ma = 20$. Solid: $Cr = 0.001$, dotted: $Cr = 0.01$, dashed: $Cr = 0.1$.

This increase also gives higher azimuthal modes the chance to play a relevant role on the instability. In particular, $m = 3$ and 4 are already the more unstable ones in a range of k when $Cr = 0.1$. Furthermore, this range increases with Ma as seen in Fig. 6b.

The corresponding critical wavenumbers presented in Fig. 7 show that the curves of the different modes are now very close to each other. Notice the presence of mode $m = 3$ for $Cr = 0.1$. This mode may also appear for larger Cr to the right of the figure for increasing Ma.

In Fig. 8 the De/Pr is larger than that of the previous figures. It is possible to appreciate the increase of the growth rate. Again mode $m = 3$, along with $m = 4$, is able to appear as the more unstable one in a range of k for $Cr = 0.1$ and $Ma = 20$. However, its growth rate, though notable, is not very different than in Fig. 6.

The curves of the critical wavenumber of all modes in Fig. 9 are also very close to each other and their increase is a little steeper than before.

Here a discussion is given about the modes intersection points. Notice that the magnitude of the wavenumber of the intersections increases with Cr. However, in the case of the intersection between

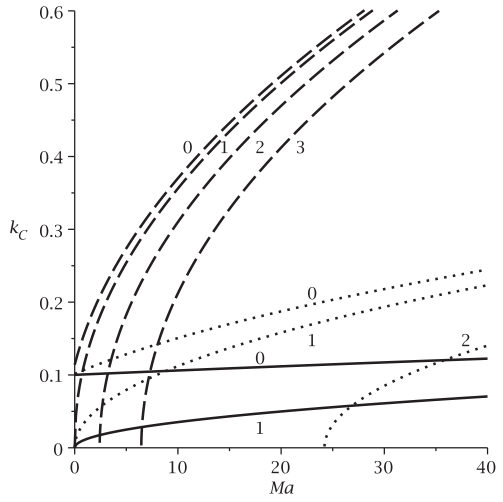

Fig. 7. k_C vs Ma. $Re = 0$. $\delta = 10$, $De/Pr = 0.01$, $Bi = 0.1$. Solid: $Cr = 0.001$, dotted: $Cr = 0.01$, dashed: $Cr = 0.1$.

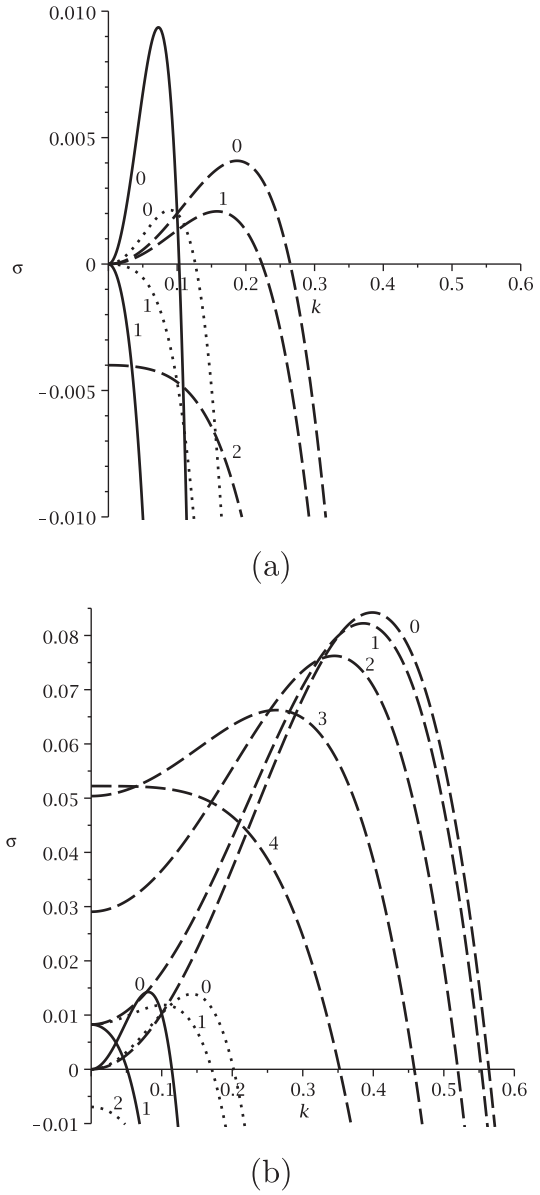

Fig. 8. σ vs k. $Re = 0$. $\delta = 10$, $De/Pr = 0.2$, $Bi = 0.1$. Fig. 8a $Ma = 0$, Fig. 8b $Ma = 20$. Solid: $Cr = 0.001$, dotted: $Cr = 0.01$, dashed: $Cr = 0.1$.

modes $m = 0$ and 1, the magnitudes of the wave numbers for $\delta = 5$ and 10 are the same for each $Cr = 0.001, 0.01$, when Ma is varied up to $Ma = 20$. Nevertheless, this is not the case at the intersection between $m = 1$ and 2 and at that of the other higher pairs of modes. Observe that for $Ma = 20$ it is possible to excite up to mode $m = 4$ as the more unstable. In general, the growth rate increases with Cr, Ma and De/Pr but decreases with δ.

4. Thermocapillary convection of a film flowing down a cylinder

This section corresponds to the description of the linear stability of a thin film flowing down the outside of a cylinder due to the action of gravity. The fixed parameters will be $Bi = 0.1$ and $S = 1$. Observe that Eq. 13 presents the ratio Ma/Pr and that the Prandtl number does not appear in another place of the equation. Therefore, the thermocapillarity parameter here will be Ma/Pr. The effect of the Reynolds number Re is of importance in this section. In normal modes $H = H_0 \exp[i(m\theta + kz + \omega t) + \sigma t]$ and assuming $\varepsilon = 1$, the phase velocity c, the growth rate σ and the critical wavenumber k_C are:

$$c = 2 + \frac{2}{3\delta}. \tag{18}$$

$$\sigma = \frac{8}{15}Rek^2 + Dek^2 + \frac{1}{3Re}\left(\frac{m^2}{\delta^2} + k^2\right)\left[\frac{S}{\delta^2} - S\left(\frac{m^2}{\delta^2} + k^2\right) + \frac{Ma}{2Pr}\frac{Bi}{(1+Bi)^2}\right]. \tag{19}$$

$$k_C^2 = -\frac{m^2}{\delta^2} + \frac{3Re}{2S}\left(\eta + \sqrt{\eta^2 - \frac{4S}{3Re}\left(\frac{8}{15}Re + De\right)\frac{m^2}{\delta^2}}\right). \tag{20}$$

where $\eta = 8Re/15 + De + S/3Re\delta^2 + MaBi/2Re(1+Bi)^2$. The critical wavenumber is obtained taking the square root of Eq. 20.

The phase velocity has the same formula as in the absence of gravity but here the velocity is made non dimensional in a different way. The growth rate now presents the Reynolds number Re in different terms of Eq. 19 and the Marangoni number is divided by the Prandtl number. It is clear that in some circumstances the Reynolds number may have a stabilizing effect when it appears in the denominator of some terms.

The growth rate of $\delta = 5$, $De = 0.01$ is shown in Fig. 10. In all the figures the numbers attached to the curves indicate the corresponding azimuthal modes. In Fig. 10a the continuous line is for $Re = 0.1$, the dotted line for $Re = 0.2$ and the dashed line for $Re = 0.3$, respectively. In Fig. 10b the continuous line is for $Re = 0.01$, the dotted line for $Re = 0.05$ and the dashed line for $Re = 0.1$, respectively. The reason to use different Reynolds number ranges is that care is taken to restrict the calculations in order to have $k < 0.6$. As can be seen in the isothermal case of Fig. 10a, the growth rate satisfies this restriction for larger Reynolds numbers than in the results with thermocapillarity. Notice that all the following Figs. 12, 14 and 16 present the same differences in the Reynolds numbers. The results presented in Figs. 10 a and b correspond to $Ma/Pr = 0$ and 2, respectively. These magnitudes are selected in order to satisfy the small wavenumber approximation.

It can be demonstrated analytically that mode $m = 0$ (the axial mode) is always the most unstable one. However, it is shown in Fig. 10 for a small viscoelastic effect that higher modes can be the more unstable ones in a range of the wavenumber. In Fig. 10a it is found that in the isothermal case the higher modes always have a lower growth rate than $m = 0$ in all the range of k. Nevertheless, thermocapillarity can stimulate higher modes and for $Ma/Pr = 2$, Fig. 10b now presents $m = 2$ as the more unstable one in a region of k for the Reynolds numbers used. Mode $m = 1$ can also be the more unstable one in another region with larger k.

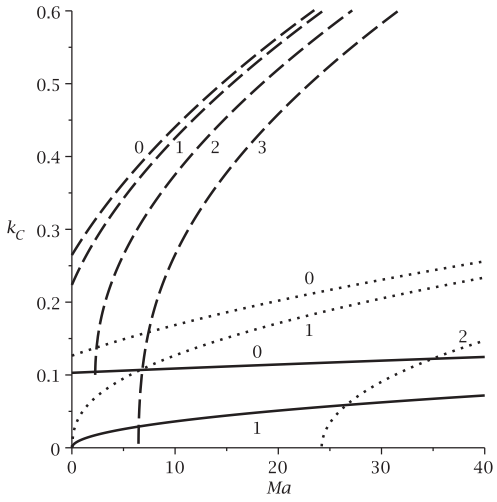

Fig. 9. k_C vs Ma. $Re = 0$. $\delta = 10$, $De/Pr = 0.2$, $Bi = 0.1$. Solid: $Cr = 0.001$, dotted: $Cr = 0.01$, dashed: $Cr = 0.1$.

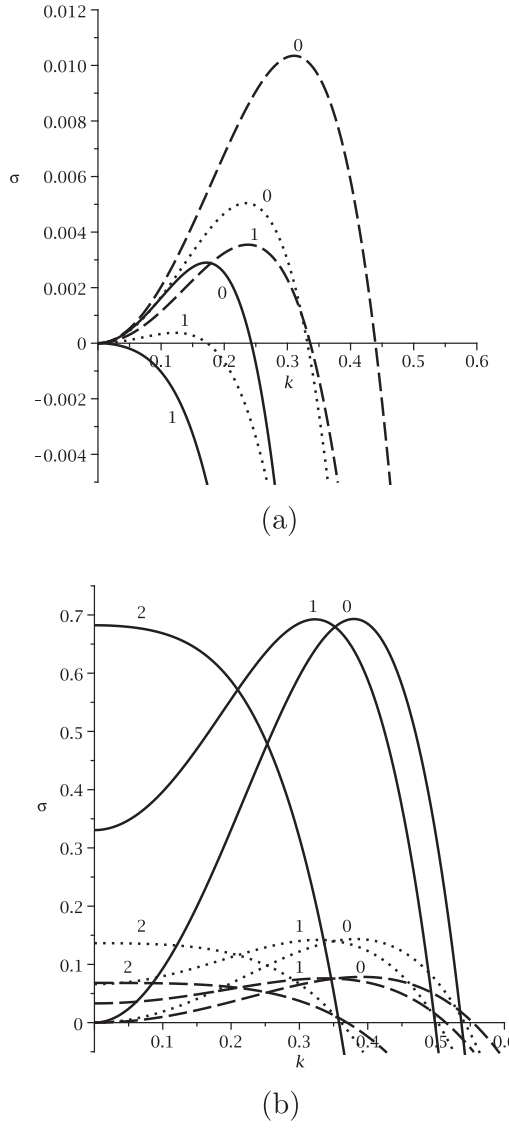

Fig. 10. σ vs k. $\delta = 5$, $De = 0.01$, $Bi = 0.1$, $S = 1$. Fig. 10a $Ma/Pr = 0$ (solid: $Re = 0.1$, dotted: $Re = 0.2$, dashed: $Re = 0.3$), Fig. 10b $Ma/Pr = 2$ (solid: $Re = 0.01$, dotted: $Re = 0.05$, dashed: $Re = 0.1$). The numbers are the azimuthal modes.

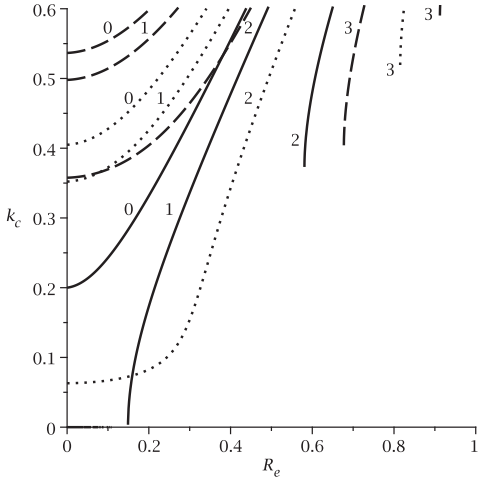

Fig. 11. k_C vs *Re*. $\delta = 5$, *De* = 0.01, *Bi* = 0.1, *S* = 1. Solid: *Ma*/*Pr* = 0, dotted: *Ma*/*Pr* = 1, dashed: *Ma*/*Pr* = 2.

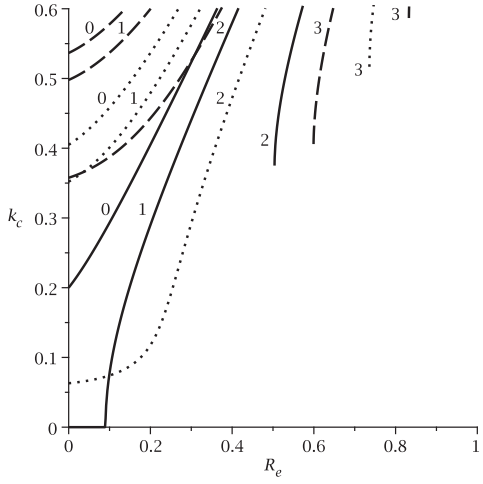

Fig. 13. k_C vs *Re*. $\delta = 5$, *De* = 0.1, *Bi* = 0.1, *S* = 1. Solid: *Ma*/*Pr* = 0, dotted: *Ma*/*Pr* = 1, dashed: *Ma*/*Pr* = 2.

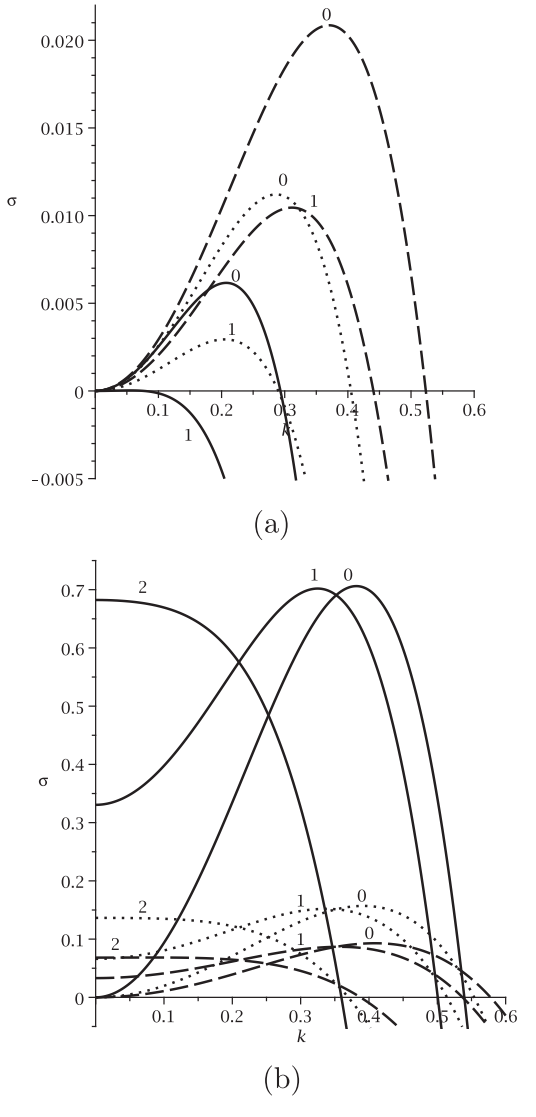

Fig. 12. σ vs k. $\delta = 5$, *De* = 0.1, *Bi* = 0.1, *S* = 1. Fig. 12a *Ma*/*Pr* = 0 (solid: *Re* = 0.1, dotted: *Re* = 0.2, dashed: *Re* = 0.3), Fig. 12b *Ma*/*Pr* = 2 (solid: *Re* = 0.01, dotted: *Re* = 0.05, dashed: *Re* = 0.1).

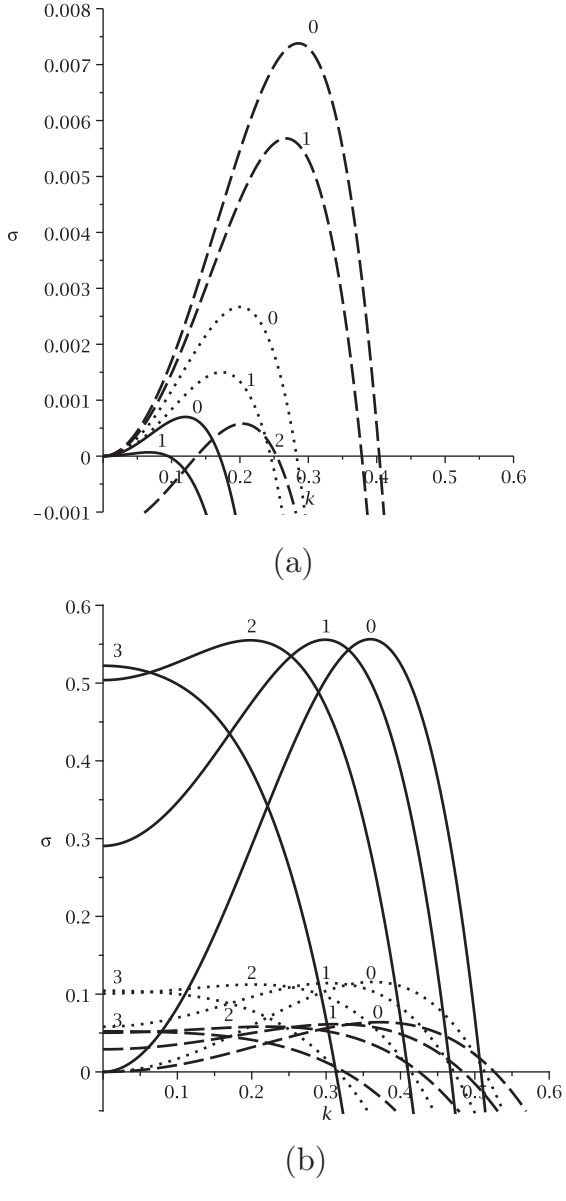

Fig. 14. σ vs k. $\delta = 10$, *De* = 0.01, *Bi* = 0.1, *S* = 1. Fig. 14a *Ma*/*Pr* = 0 (solid: *Re* = 0.1, dotted: *Re* = 0.2, dashed: *Re* = 0.3), Fig. 14b *Ma*/*Pr* = 2 (solid: *Re* = 0.01, dotted: *Re* = 0.05, dashed: *Re* = 0.1).

In Fig. 10 there are a number of intersections between the pairs of curves of the azimuthal modes. As can be seen, the wavenumber of the intersection does not depend on the Reynolds number but only on the parameter Ma/Pr. The reason is that the terms independent of m, including the viscoelastic one, disappear when subtracting the growth rates of the intersecting modes to calculate k. Only the thermocapillary terms remain. Still, the corresponding growth rate at the intersection has an important dependence on De and Re.

The critical wavenumber is plotted in Fig. 11 against Re for three values of Ma/Pr. It is clear that k_C increases very fast with Re. Some curves are cut for lower k_C because of the negative magnitude of the radicand in the definition of k_C Eq. 20. Higher modes start to appear but they are approaching the limits of the small wavenumber approximation.

In Fig. 12 the Deborah number increases ten times. It is clear in Fig. 12a that in the isothermal case this produces an important change in the growth rate with respect to Fig. 10a. But there is a small increase in Fig. 12b. Therefore, thermocapillarity here stands out more than viscoelasticity. The growth of k_C with Re is shown in Fig. 13. It is found that this is more steep than in Fig. 11. Thus higher modes are able to appear for smaller Reynolds numbers.

The radius is larger in Fig. 14. This affects considerably the growth rate in both the isothermal and non isothermal flows. Nevertheless, the azimuthal mode $m = 3$ is able to appear as the more unstable one in a range of the wavenumber for the two magnitudes of Ma/Pr. Another consequence of increasing the radius is that the maximum of mode $m = 2$ is displaced to right in contrast with that of $m = 0$ and 1, which is small. It is interesting that the maxima of $m = 0$, 1 and 2 decrease in this order and that they are very close to each other, contrary to $m = 3$.

Fig. 15 shows that k_C increases with Re even faster than before. The mode $m = 3$ has more presence with respect to Re inside the small wavenumber approximation.

The Deborah number now is twenty times larger in Fig. 16. The growth rate increases considerably in Fig. 16a for the isothermal problem. There, more azimuthal modes are excited by viscoelasticity. The influence of thermocapillarity is clear in Fig. 16b where the growth rates differ with respect to those of Fig. 14. It is important to point out that now the magnitude differences among the growth rate maxima of modes $m = 0$, 1, 2 and 3 are notable for the two magnitudes of Ma/Pr.

The curves of criticality are presented in Fig. 17. It is found that they show the steepest growth among the figures presented before

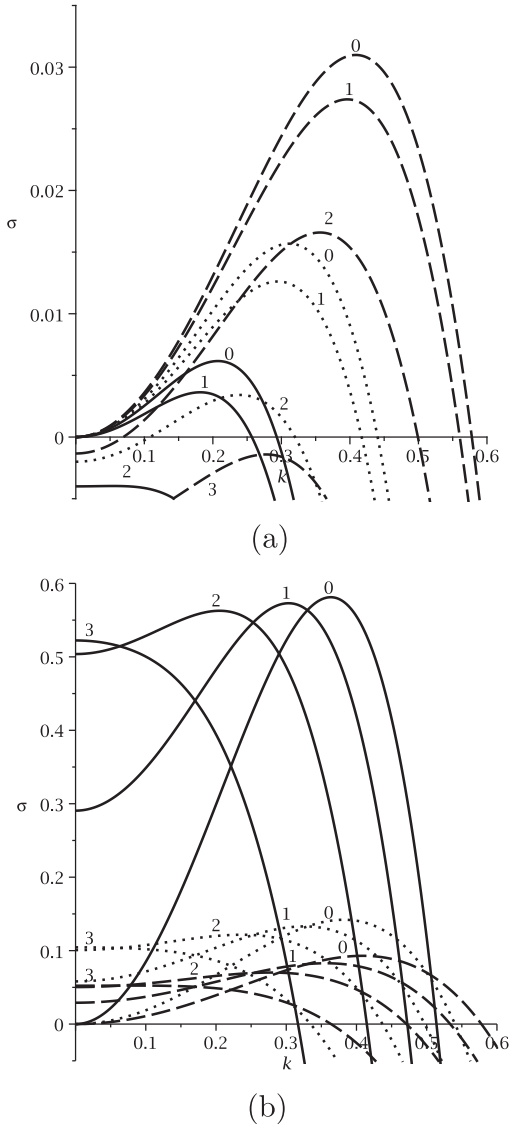

Fig. 16. σ vs k. $\delta = 10$, $De = 0.2$, $Bi = 0.1$, $S = 1$. Fig. 16a $Ma/Pr = 0$ (solid: $Re = 0.1$, dotted: $Re = 0.2$, dashed: $Re = 0.3$), Fig. 16b $Ma/Pr = 2$ (solid: $Re = 0.01$, dotted: $Re = 0.05$, dashed: $Re = 0.1$).

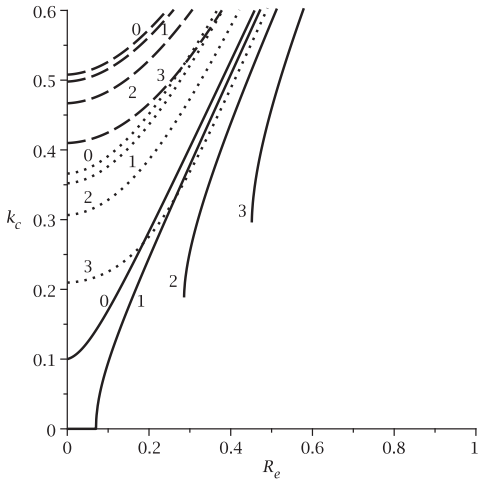

Fig. 15. k_C vs Re. $\delta = 10$, $De = 0.01$, $Bi = 0.1$, $S = 1$. Solid: $Ma/Pr = 0$, dotted: $Ma/Pr = 1$, dashed: $Ma/Pr = 2$.

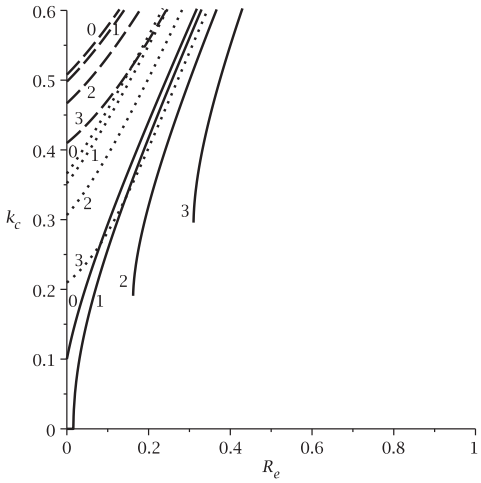

Fig. 17. k_C vs Re. $\delta = 10$, $De = 0.2$, $Bi = 0.1$, $S = 1$. Solid: $Ma/Pr = 0$, dotted: $Ma/Pr = 1$, dashed: $Ma/Pr = 2$.

for $Re > 0$. Higher azimuthal modes have a larger k_C range inside the small wavenumber approximation.

The results of modes intersections are discussed here. Notice that the magnitudes of the intersection wavenumbers do not change with Re, δ and De. An appreciable change occurs with Ma/Pr for the same intersecting modes. Since higher modes only appear for large δ, this can only be seen for two different magnitudes of De. For $Ma/Pr < 2$ and $\delta = 5$ it is only possible to excite up to $m = 1$, but for $\delta = 10$ up to $m = 3$. When $Ma/Pr = 2$ and $\delta = 5$ it is possible to excite up to mode $m = 2$ and for $\delta = 10$ up to $m = 3$. Note that the growth rates decrease with Re and δ and increase with Ma/Pr and De.

5. Conclusions

In the absence of gravity it is found that the most unstable mode is the axial one, that is $m = 0$. The results bring about the possibility of controlling the azimuthal modes as the more unstable ones by means of the wavenumber as done theoretically in [21,20] for example. In the isothermal case viscoelasticity is only able to excite the azimuthal modes by increasing their growth rates, as shown in [37]. Here, it is found that an increase of the crispation number in the thermocapillary flow makes it easier to open a wavenumber range where azimuthal modes are the more unstable. As a general rule, this always occurs in a range where the wavenumber is smaller than that corresponding to the maximum growth rate of $m = 0$. Some modes may have their maximum at $k = 0$ and others at $k > 0$, depending on the parameters. A notable difference in the number of excited unstable modes is made by the radius of the cylinder. The wavenumber of the intersections between two modes is constant with respect to those parameters which do not multiply the mode number m in the intersection formula.

The problem of the vertical cylinder under gravity also shows interesting results. When $Ma = 0$ the growth rate of the azimuthal modes is always smaller than that of $m = 0$ in all the unstable range of the wavenumber. Their growth rate in the range of k behaves as $\sigma_{m=0} > \sigma_{m=1} > \sigma_{m=2} > \cdots$, etc. Also in the non isothermal problem $m = 0$ is always the most unstable one. The maximum growth rates of the different modes satisfy the inequalities $\sigma^{max}_{m=0} > \sigma^{max}_{m=1} > \sigma^{max}_{m=2} > \cdots$, etc. Nevertheless, other modes can be the more unstable and behave for example in a range of k as $\sigma_{m=3} > \sigma_{m=2} > \sigma_{m=1} > \sigma_{m=0} > \sigma_{m=4} > \cdots$ and in another range of k as $\sigma_{m=2} > \sigma_{m=3} > \sigma_{m=1} > \sigma_{m=0} > \sigma_{m=4} > \cdots$, etc. In this case the wavenumber at the intersection remains constant with respect to those parameters which are not multiplied by the mode number m in the equation calculated for the intersections. However, the corresponding growth rate always depends on all the parameters involved in the problem. Tables with numerical modes intersection data are available upon request.

Despite the large number of parameters involved, it was possible to review a series of characteristics of the linear stability of the two complex flows investigated. Next it is of interest to explore the nonlinear instability.

Conflict of interest

The authors wish to confirm that there are no known conflicts of interest associated with this publication and there has been no significant financial support for this work that could have influenced its outcome.

Acknowledgments

The authors would like to thank, Joaquín Morales, Cain González, Raúl Reyes, Alberto López, Ma. Teresa Vázquez and Oralia Jiménez for technical support.

References

[1] J.R.A. Pearson, On convection cells induced by surface tension, J. Fluid Mech. 4 (1958) 482–500.
[2] L.E. Scriven, C.V. Sternling, On cellular convection driven by surface-tension gradients: effects of means surface tension and surface viscosity, J. Fluid Mech. 19 (1964) 321–340.
[3] M. Takashima, Surface tension driven instability in a horizontal liquid layer with a deformable free surface. I. Stationary convection, J. Phys. Soc. Jpn. 50 (1981) 2745–2750.
[4] M. Takashima, Surface tension driven instability in a horizontal liquid layer with a deformable free surface. II. Overstability, J. Phys. Soc. Jpn. 50 (1981) 2751–2756.
[5] C.L. Mctaggart, Convection driven by concentration and temperature dependent surface tension, J. Fluid Mech. 134 (1983) 301–310.
[6] R.B. Bird, O. Hassager, Dynamics of Polymeric Liquids, Vol. 1: Fluid Mechanics, second ed., Wiley-Interscience, New York, 1987.
[7] L.A. Dávalos-Orozco Viscoelastic natural convection, in: J. de Vicente (Ed.), Viscoelasticity – From Theory to Biological Applications, Intech, Rijeka, 2012, pp. 3–32 (open access).
[8] I. Pérez-Reyes, L.A. Dávalos-Orozco, Effect of thermal conductivity and thickness of the walls in the convection of a viscoelastic Maxwell fluid layer, Int J. Heat Mass Transfer 54 (2011) 5020–5029.
[9] I. Pérez-Reyes, L.A. Dávalos-Orozco, Vorticity effects in the non-linear long wavelength convective instability of a viscoelastic fluid layer, J. Non-Newtonian Fluid Mech. 208–209 (2014) 18–26.
[10] D. Getachew, S. Rosenblat, Thermocapillary instability of a viscoelastic liquid layer, Acta Mech. 55 (1985) 137–149.
[11] S.R.D. Wilson, Growth rates of the Marangoni instability in a layer of elastic fluid, Rheol. Acta 34 (1995) 601–605.
[12] P.G. Siddheshwar, G.N. Sekhar, G. Jayalatha, Surface tension driven convection in viscoelastic liquids with thermorheological effect, Int. Commun. Heat Mass Transfer 38 (2011) 468–473.
[13] I.J. Hernández-Hernández, L.A. Dávalos-Orozco, Competition between stationary and oscillatory viscoelastic thermocapillary convection of a film coating a thick wall, Int. J. Therm. Sci. 89 (2015) 164–173.
[14] S.W. Joo, P.G., S.H. Davis, S.G. Bankoff, A mechanism for rivulet formation in heated falling films, J. Fluid Mech. 321 (1996) 279–298.
[15] B. Ramaswamy, S. Krishnamoorthy, S.W. Joo, Three-dimensional simulation of instabilities and rivulet formation in heated falling films, J. Comput. Phys. 131 (1997) 70–88.
[16] S.W. Joo, P.G., S.H. Davis, S.G. Bankoff, Long-wave instabilities of heated falling films: two-dimensional theory of uniform layers, J. fluid Mech. 230 (1991) 117–148.
[17] L.A. Dávalos-Orozco, Stability of thin liquid films falling down isothermal and nonisothermal walls, Interfacial Phenom. Heat Transfer 1 (2013) 93–138.
[18] S.W. Joo, The stability and nonlinear flow developments of a viscoelastic draining film with shear thinning, J. Non-Newton. Fluid Mech. 51 (1994) 125–140.
[19] F. Kang, K.P. Chen, Nonlinear elastic instability of gravity-driven flow of a thin viscoelastic film down an inclined plane, J. Non-Newton. Fluid Mech. 57 (1995) 243–252.
[20] L.A. Dávalos-Orozco, Stability of thin viscoelastic films falling down wavy walls, Interfacial Phenom. Heat Transfer 1 (2013) 301–315.
[21] L.A. Dávalos-Orozco, Nonlinear instability of a thin liquid film falling down a smoothly deformed surface, Phys. Fluids 19 (2007) 074103.
[22] T. Shlang, G.I. Sivashinsky, Irregular flow of a liquid film down a vertical column, J. Phys. (France) 43 (1982) 459–466.
[23] M. Ozawa, T. Ami, H. Umekawa, R. Matsumoto, T. Hara, Forced flow boiling of carbon dioxide in horizontal mini-channel, Int. J. Therm. Sci. 50 (2011) 296–308.
[24] A. Sur, D. Liu, Adiabatic Air–Water two-phase flow in circular microchannels, Int. J. Therm. Sci. 53 (2012) 18–34.
[25] L.A. Dávalos-Orozco, G. Ruiz-Chavarría, Hydrodynamics instability of a fluid layer flowing down a rotating cylinder, Phys. Fluids A 5 (1993) 2390–2404.
[26] G. Ruiz-Chavarría, L.A. Dávalos-Orozco, Stability of a liquid film flowing down a rotating cylinder subject to azimuthal disturbances, J. Phys. II (France) 9 (1996) 1219–1227.
[27] G. Ruiz-Chavarría, L.A. Dávalos-Orozco, Azimuthal and streamwise disturbances in a fluid flowing down a rotating cylinder, Phys. Fluids 9 (1997) 2899–2908.
[28] R. Bertossi, N. Guilhem, V. Ayel, C. Romestant, Y. Bertin, Modeling of heat and mass transfer in the liquid film of rotating heat pipes, Int. J. Therm. Sci. 52 (2012) 40–49.
[29] L.A. Dávalos-Orozco, E. Vázquez-Luis, Instability of the interface between two inviscid fluids inside a rotating annulus in the absence of gravity, Phys. Fluids 15 (2003) 2728–2739.
[30] R. Ben Radhia, J.P. Corriou, S. Harmand, S. Ben Jabrallah, Numerical study of evaporation in a vertical annulus heated at the inner wall, Int. J. Therm. Sci. 50 (2011) 1996–2005.
[31] L.A. Dávalos-Orozco, X.-Y. You, Three-dimensional instability of a liquid layer flowing down a heated vertical cylinder, Phys. Fluids 12 (2000) 2198–2209.
[32] P.J. Cheng, K.C. Liu, Stability analysis of the thin power-law liquid film flowing down a vertical cylinder, Trans. Can. Soc. Mech. Eng. 30 (2006) 81–96.

[33] P.J. Cheng, K.C. Liu, Longwave perturbation method to investigate nonlinear stability of the thin power-law liquid film flowing down on a vertical cylinder, J. Mech. 24 (2008) 241–252.
[34] P.J. Cheng, K.C. Liu, Hydromagnetic instability of a power-law liquid film flowing down a vertical cylinder using numerical approximation approach techniques, Appl. Math. Model. 33 (2009) 1904–1914.
[35] P.J. Cheng, C.K. Chen, H.Y. Lai, Nonlinear stability analysis of thin viscoelastic film flow traveling down along a vertical cylinder, Nonlinear Dyn. 24 (2001) 305–332.
[36] P.J. Cheng, D.T.W. Lin, Surface waves in a viscoelastic magnetic fluid film flow down a vertical cylinder, Int. J. Eng. Sci. 45 (2007) 905–922.
[37] M. Moctezuma-Sánchez, L.A. Dávalos-Orozco, Linear three dimensional instability of viscoelastic fluid layers flowing down cylindrical walls, Microgravity Sci. Technol. 20 (2008) 161–164.
[38] A.L. Frenkel, On evolution equations for thin films down solid surfaces, Phys. Fluids A 5 (1993) 2342–2347.